DJS Vol. 46(1) (2023) pp. 23- 35 ISSN: 1012-5965

Delta Journal of Science

Available online at **https://djs.journals.ekb.eg/**

Research Article **PHYSICS**

Thermal and electrical properties of Cr-doped Cd-Cu nanoferrites samples

A. W. Awad[1*], R. E. El shater[1], H. H. El-Bahnasawy[2], T. M. Meaz[1]

[1] Physics department, faculty of science, Tanta University, 31527, Egypt
[2] Physics Department, Faculty of Science, Al-Azhar University, Nasr City 11884, Cairo, Egypt

Corresponding author : Ahmed Awad **e-mail:** ahmed_awad@science.tanta.edu.eg **&** awawad19@gmail.com

Recived:16/1/2023 Accepted: 1/2/2023

KEY WORDS

Ferrites, Co-precipitation, TGA, DC conductivity

ABSTRACT

Cr substituted Cd-Cu nanoferrite materials ($Cd_{0.5}Cu_{0.5}Cr_xFe_{2-x}O_4$ with x = 0.0, 0.05, 0.1, 0.2, 0.4, and 0.8) were successfully fabricated by the co-precipitation technique. XRD, TGA, and DC electrical measurements were utilized to identify the synthesized nano samples. According to an XRD analysis, the obtained samples are cubic structures with space group Fd3m. The estimated crystallite size by the Scherrer formula is in the range of 14.8-22.6 nm. However, the SEM measurements revealed that the nanoparticles' estimated particle sizes ranged from 37.5 to 52.5 nm. As indicated by TGA graphs, the average decomposition energies of the four stages of the weight loss of decomposition are 1.39, 6.53, 39.14, and 40.21 (KJ/mol). The room temperature conductivity decreased gradually from 7.34×10^{-7} Ω^{-1} cm^{-1} for the Cr00 sample to 2.24×10^{-8} Ω^{-1} cm^{-1} for the Cr80 sample, while the values of activation energy were found in the range from 0.349-0.407 eV. The temperature-dependent of dc-electrical conductivity for all the samples exhibits semiconductor-like behavior. As a result, Cd-Cu doped materials may be suitable for limiting eddy current losses.

Introduction

Magnetic nanoparticles are crucial in various technology fields, such as power transformers, magnetic resonance imaging, magneto-optical displays, sensors, media recording, biomedicine, etc. **(Jadoun *et al.,* 2018)**. Nanoferrites are materials that have drawn much attention because they have unique physical, chemical, biological, magnetic, and electrical properties, among other magnetic materials. The intrinsic properties of ferrites are significantly influenced by chemical structure, sample preparation parameters, sintering temperature, cation distribution, and elemental doping **(Amer *et al.,* 2017)**. The majority of articles that have been published have discussed how physical and chemical properties vary based on synthesis methods, doping processes, and ionic radii of cations **(Amer *et al.,* 2017)**. An important factor impacting the chemistry and physical properties of the nano ferrites is the distribution of cations among the tetrahedral sites (A-sites) and octahedral sites (B-sites).

The spinel structure has 56 ions; 8 of the 32 accessible cations occupy the A-sites, and 16 of the 64 accessible cations occupy the B-sites, where 32 of these atoms are oxygen anions. The typical spinel compound's structural formula is as follows: MFe_2O_4 may be distributed as $(M_{1-x}Fe_x)_A[M_xFe_{2-x}]_BO_4$ where A and B are quantities that indicate the normal occupation of A- and B-sites, respectively, and x is the inversion ratio. A mixed spinel has x equal to 1, an inverse spinel has x equal to 0, and a normal spinel has x equal to 0 **(Hashim *et al.,* 2014)**.

There are several different types of ferrites with normal spinel structures, such as MFe_2O_4 ($M_A[Fe_2]_BO_4$), here M is Zn, Cd metal ions, the tetrahedral position is occupied by metal ions, whereas the octahedral position is occupied by iron ions **(Hashim *et al.,* 2014)**, **(Gupta *et al.,* 2018)**. Ferrites with inverse spinel-type structures $Fe[MFe]O_4$, where M is Ni, Co, Fe, Mn, and Cu **(Naik *et al.,* 2013)**. It is usually known that Fe^{3+} ions may occupy both the tetrahedral and octahedral sites, while Cr^{3+} ions primarily occupy the octahedral sites of cubic spinel's **(Amer *et al.,* 2017)**, **(Mansour, Abdo and Alwan, 2018)**. The copper ferrite $CuFe_2O_4$ is known to be inverse spinel $(Fe)_A[CuFe]_BO_4$, based on the synthesis and cooling techniques **(Hashim *et al.,* 2013)**. The $Cd_{0.5}Cu_{0.5}Fe_2O_4$ is mixed spinel ferrites **(Ghasemi *et al.,* 2020)**. As a result, it is important to investigate the influence of Cr^{3+} insertion on the structural and

thermal/electrical properties of Cd - Cu nano ferrites.

Polaron hopping models are a key factor in determining how ferrites conduct electricity. The density, porosity, particle size, chemical composition, and crystal structure of ferrites all significantly impact their electrical resistivity. Due to a reduction in grain boundary resistance, the temperature rises to cause a drop in resistivity. The polarization phenomenon and the behavior of localized electric charge carriers are reflected in the electrical properties **(Supriya, Kumar and Kar, 2017)**. Cr-doped magnetite's thermal and magnetic characteristics have been studied (**Amer *et al.*, 2017)**. They revealed that lattice constant and grain size decreased with increasing Cr^{3+} ion concentration, and the TG curves indicated three phases of the decomposition process with net weight losses ranging from 19% to 33%. The structural and electrical aspects of Zn^{2+} doped $MgFeCrO_4$ nanoparticles **(Khalaf *et al.*, 2016)** have been studied. The outcome of this study was that the progressive rise of the Zn^{2+} concentration results in a gradual transition from the mixed to normal spinel structure.

The controlled manufacturing of ferrite nanoparticles allows for tuning their magnetic characteristics. The co-precipitation technique **(Amer *et al.*, 2017)**, microemulsion technique, sol-gel auto-combustion technique **(Mansour, Abdo and Alwan, 2018)**, and hydrothermal process **(Wang *et al.*, 2015)** are all employed to synthesize spinel ferrites nanoparticles. According to time and energy utilization, the co-precipitation strategy is quite efficient. A sizeable portion of the final result is generated affordable compared to other procedures with great uniformity **(El-Shater, El Shimy and Assar, 2020)**. This work aims to synthesize Cr-doped $Cd_{0.5}$ $Cu_{0.5}$ ferrite nano samples and investigate the impact of changing the Cr^{3+} ion level on their properties. The authors believe that investigating the properties of these nano sample may be beneficial for various interesting applications.

Experimental works

Materials and method

Nano-crystalline chromium doped cadmium copper ferrites with the stoichiometric formula $Cd_{0.5}Cu_{0.5}Cr_xFe_{2-x}O_4$ (x = 0.0, 0.05, 0.1, 0.2, 0.4, and 0.8) were prepared by the co-precipitation process. Analytical grade Cadmium nitrate $[Cd(No_3)_2.4H_2O]$ Copper nitrate $[Cu(NO_3)_2.4H_2O]$, chromium nitrate $[Cr(NO_3)_3.9H_2O]$ and iron nitrate $[Fe(No_3)_3.9H_2O]$ as starting materials were mixed initially at a molar ratio of 1:2 M. The molarities of divalent metals

were 0.2 M, and the molarities of trivalent metals were 0.4 M. Using a magnetic stirrer, the metal nitrates were dissolved in 125 mL of distilled water for all samples, and 3M of sodium hydroxide (NaOH) was dissolved in the mixture. For two hours, the solution was warmed up to 90°C until precipitation occurred. The precipitations were washed numerous times in deionized water to eliminate unwanted salt residuals before being dried in an oven at 100°C overnight, then crushed to a fine powder in an agate mortar **(Vadivel *et al.*, 2014)**. Table (1) represents the names of synthesized samples.

Table (1): The symbols of synthesized samples

Sample	Symbol
$Cd_{0.5}Cu_{0.5}Cr_{0.00}Fe_2O_4$	Cr00
$Cd_{0.5}Cu_{0.5}Cr_{0.05}Fe_2O_4$	Cr05
$Cd_{0.5}Cu_{0.5}Cr_{0.10}Fe_2O_4$	Cr10
$Cd_{0.5}Cu_{0.5}Cr_{0.20}Fe_2O_4$	Cr20
$Cd_{0.5}Cu_{0.5}Cr_{0.40}Fe_2O_4$	Cr40
$Cd_{0.5}Cu_{0.5}Cr_{0.80}Fe_2O_4$	Cr80

Materials identifications

The prepared samples were characterized for their crystalline structure using X-Ray Diffraction using the model PANalytical (X'pert Pro, Netherlands), equipped with a high-intensity Cu k radiation source (= 0.154 nm, 40 mA, 40 kV) in the 2θ range 10°-80°.

The morphology of the investigated nano samples was determined, and surface morphology was accomplished by using field emission scanning electron microscopy (FESEM) images that were collected utilizing Hitachi S-4800 scanning electron microscope. In order to understand the decomposition behavior of the samples' precursors, TG analysis was carried out. Thermogravimetric analysis (TGA) of the spinel ferrites was performed by utilizing Perkin Elmer (Japan) from ambient temperature (RT) to 800 ºC at a heating rate of 10°/min when there is an airflow atmosphere. A Keithley multimeter was used to test the samples' dc electrical conductivity as a function of temperature.

The samples' dc electrical conductivity was measured as a function of temperature by a Keithley multimeter using the two-probe method. By using the Arrhenius relationship in the connection between dc conductivity and temperature **(Assar and Abosheiasha, 2015)**: $\sigma_{dc} = \sigma_o \exp(-E_a/KT)$ where σ_o is a pre-exponential constant, E_a is the activation energy for dc conduction, K is Boltzmann's constant = 8.617 × 10^5 eVK^{-1} and T is the absolute temperature.

Result and discussion

X-ray diffraction analysis

The prepared samples' structural properties were determined using the x-ray diffraction technique. The x-ray diffraction patterns of the as-prepared samples are shown in Fig. 1. The most intense peaks in the complete nano ferrites were indexed as (220), (311), (222), (400), (422), (511) and (440) were found to be closely matched with the single phase cubic spinel structure. [compared with JCPDS card No. 00-022-1086] and confirmed the Fd3m space group with FCC structure **(Uday Bhasker *et al.*, 2016)**.

The peak (311) is almost the spinel ferrites' main distinctive peak **(Yadav *et al.*, 2019)**. As stated by Bragg's relation, the inter-planar distance (d) is related to the cubic structure's lattice constant (a) as follows:

$$a = d(h^2+h^2+l^2)^{1/2} \quad (1)$$

Where h, k, and l are the miller indices of the planes associated with the characteristic peak.

The structural properties of the nano-samples are mentioned in Table 2. It is obvious that when the concentration of Cr^{3+} increases, the lattice parameter of the samples decreases. The lattice parameter has been estimated using the diffraction patterns, which decrease with increasing Cr^{3+} ions substitution in the prepared samples. The drop in lattice parameter is ascribed to the substitution of smaller Cr^{3+} (0.6 Å) ions for larger Fe^{3+} (0.64 Å) ions **(Mansour, Abdo and Alwan, 2018)**.

The experimental density D_{exp} is accurately determined using geometrical methods Eq. 2, which is accomplished by determining each pellet's mass, diameter, and thickness. The X-ray density D_x is calculated from the lattice parameter values using the formula in Eq. 3.

$$D_{exp} = \frac{m}{\pi r^2 t} \quad (2)$$

$$D_x = \frac{ZM}{N_A a^3} \quad (3)$$

In the case of spinel ferrites, Z is the number of molecules per unit cell (Z=8), M is the sample's molecular weight (g/mole), N_A is the Avogadro's number (6.023×10^{23} atoms/mole), and m, r, and t are the mass, radius, and thickness of each pellet, respectively. When Cr is substituted, the X-ray density D_x rises. Since the lattice constant and x-ray density exhibit an inverse connection, the increase in x-ray density was brought on by the decrease in the lattice constant (Ashiq *et al.*, 2012).

Each pellet's porosity (P) is calculated using the following formula in Eq. 4

$$P = \frac{D_x - D_{exp}}{D_x} \quad (4)$$

The porosity *P* of the compositions is inversely related to the density.

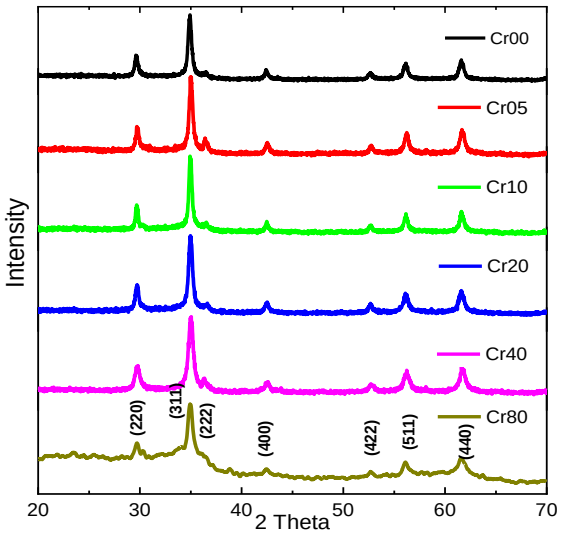

Fig. (1): XRD patterns of $Cd_{0.5}Cu_{0.5}Cr_xFe_{2-x}O_4$ nanoferrite samples

Table (2): The calculated XRD parameters of $Cd_{0.5}Cu_{0.5}Cr_xFe_{2-x}O_4$ nano ferrites samples: lattice parameter (*a*), x-ray density (D_x), experimental density (D_{exp}), porosity (*P*).

Sample	*a*	D_x	D_{exp}	*P*
	Å	g/cm^3	g/cm^3	(%)
Cr00	8.517	5.670	2.56	0.548
Cr05	8.507	5.689	2.36	0.585
Cr10	8.503	5.699	2.51	0.560
Cr20	8.500	5.702	2.32	0.592
Cr40	8.492	5.689	2.25	0.604
Cr80	8.490	5.622	2.23	0.603

Thermo-Gravimetric Analysis (TGA)

Thermo-Gravimetric Analysis (TGA) is an appropriate and effective technique for determining the degree of dopants and water content in ferrites. It is also helpful for determining the thermal deterioration profile and thermal stability. The mass loss profile may be used to calculate the amount of degraded matter at each curve step **(Gul H *et al.*, 2018)**. The TGA behavior of Cd - Cu nano ferrites doped with different Cr concentrations are displayed in Fig. 2. The TGA curves for the samples exhibit three distinct stages of weight loss throughout three temperature ranges, from room temperature to 799°C at a heating rate of 10 C/min.

The first stage of weight loss is seen in the temperature range of RT to 100°C, and it involves a significant weight loss due to absorbed water evaporation and the dryness of the OH group in the composite structure. According to the breakdown of nitrate combustion, the second weight loss stage is seen in the 337 to 369°C range **(El-Shater, 2018)**. The third stage of weight reduction is noticed to begin above 567°C, demonstrating that thermal degradation has been finished. Finally, thermally stable ferrite powder is obtained **(Kaur *et al.*, 2019)**. All the nano ferrites showed complete decomposition at temperatures above 515 - 627°C.

From Table 3, the initial weight reduction stage is 2.55, 2.9, 2.7, 3.63, 3.09, and 6.14% for samples, respectively. The second weight reduction stage is from 5.17% - 12.27%,

with increasing Cr content. The TGA curve first reveals weight reduction, and its analysis shows thermal degradation of the Chromium ferrite nanomaterials under consideration. TGA is used to calculate the decomposition energy E_d. Understanding these variables is important for analyzing thermal stability and, consequently, the behavior of materials at high temperatures. Horowitz and Metzger's approach may be used to extract the pyrolysis parameter and compute the E_d of degradation. According to this method **(Gul H *et al.*, 2018)**.

$$ln[ln\{(W_0 - W_f)/(W_t - W_f)\}] = E_d \theta / RT_s^2 \quad (5)$$

where W_0 represents the sample's weight at the beginning of the experiment, W_f is the experiment's final weight, and W_t is the sample's weight when the temperature rises. R is the universal gas constant, while E_d is the decomposition energy, and T_s is the reference temperature which can be determined from the following equations:

$$(W_t - W_f)/(W_0 - W_f) = 1/e \quad (6)$$

$$\theta = T - T_s \quad (7)$$

As a result, the decomposition energy is calculated using the slope of the plot, where $ln[ln\{(W_0 - W_f)/(W_t - W_f)\}]$ verses θ. The values of T_s and E_d for the four phases of spinel breakdown ferrites were registered in Table 3. For the four phases, the average values of E_d are 1.39, 6.53, 39.14, and 40.21 (KJ/mol).

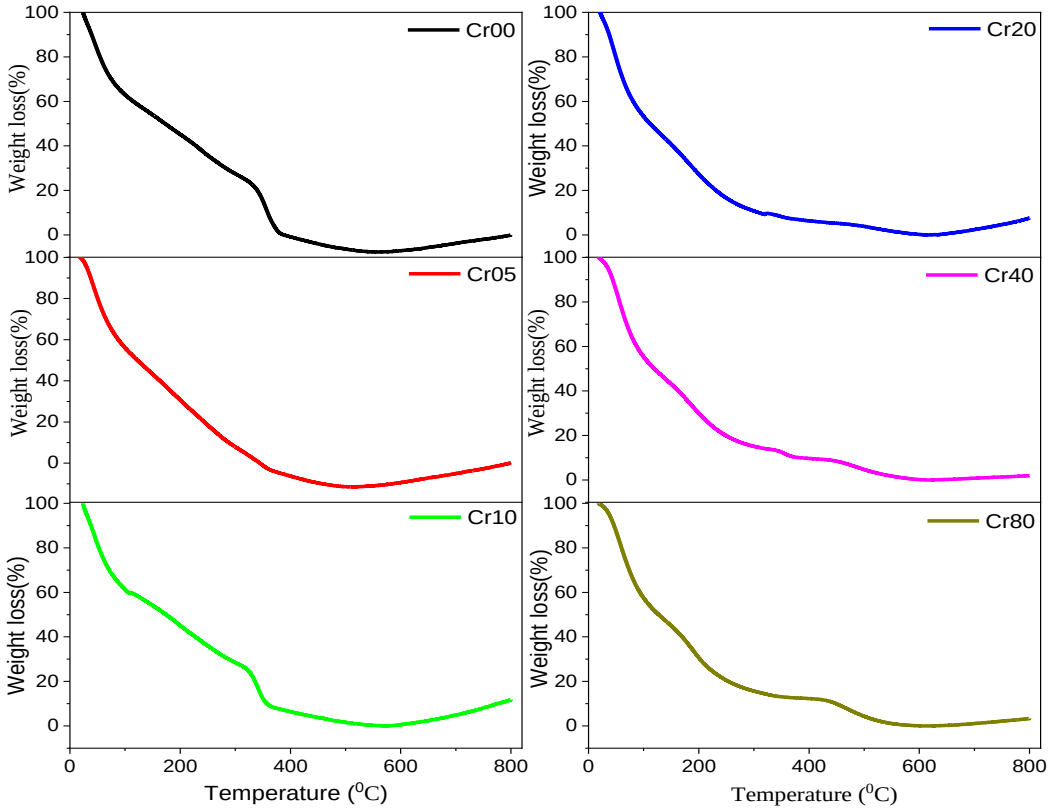

Fig. (2): TGA curves of $Cd_{0.5}Cu_{0.5}Cr_xFe_{2-x}O_4$ nanoferrite samples

Table (3): TGA transition temperature T_s in (°C) and decomposition energy E_d in (kJ/mol) for $Cd_{0.5}Cu_{0.5}Cr_xFe_{2-x}O_4$ nano ferrites samples.

Sample	Stage$_1$		Stage$_2$		Stage$_3$		Stage$_4$		Stage$_5$	
	T_s	E_d	T_s	E_d	T_s	E_d	T_s	E_d	T_s	E_d
Cr00	54.613	1.4	225.92	2.78	358.33	17.6	393.42	74.5	787.29	390
Cr05	59.953	1.4	247.02	6.56	354	31.36	424.01	32.1	716.98	52.7
Cr10	60.972	1.24	233.37	7.91	343.42	96	459.41	27	742.66	79.7
Cr20	58.86	1.59	185.82	5.84	286.46	57.4	509.63	22.8	752.47	93.6
Cr40	72.79	1.45	216.9	4.76	393.49	16.9	523.92	42.0	738.65	75.9
Cr80	82.9	1.26	219.88	6.62	432.01	15.6	509.25	42.9	748.49	94.6

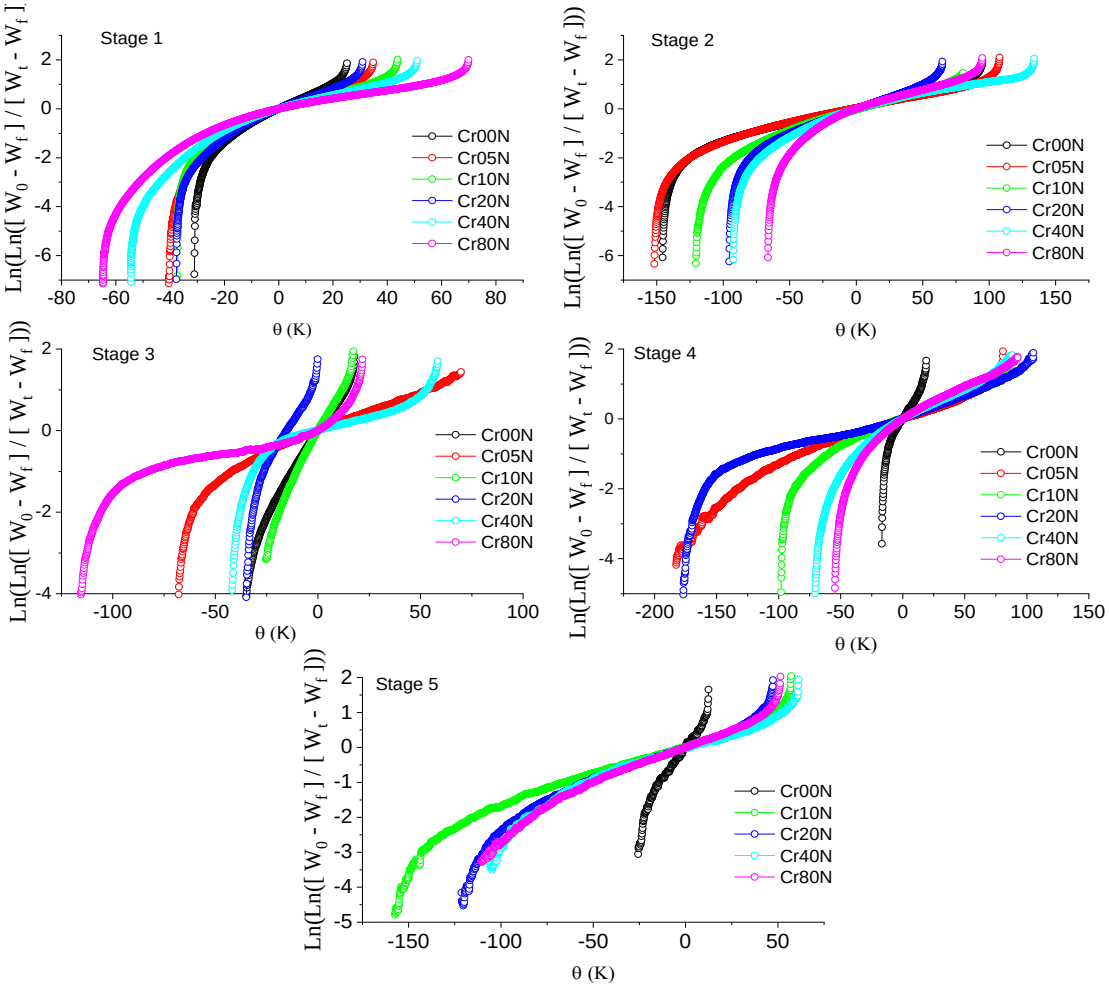

Fig. (3): Plots of activation energy of $Cd_{0.5}Cu_{0.5}Cr_xFe_{2-x}O_4$ nanoferrite samples

Scanning electron microscope

The materials' morphology significantly affects their magnetic and electrical characteristics. The scanning electron microscope was utilized to investigate the surface of the samples and correlate it with the behavior of their characteristics. The SEM pictures of the current samples are shown in Fig. 4. The particle agglomeration phenomenon is allowed by the surface activity, demonstrating that all the particles are thoroughly cemented. The magnetic interactions among particle surfaces may cause the observed particle agglomeration **(El-Shater, El Shimy and Assar, 2020)**. The increased doping ion concentration causes high agglomeration and clustering, which may be induced by oxygen vacancies and porosity that restrict grain dispersion **(Lokesha *et al.*, 2021)**.

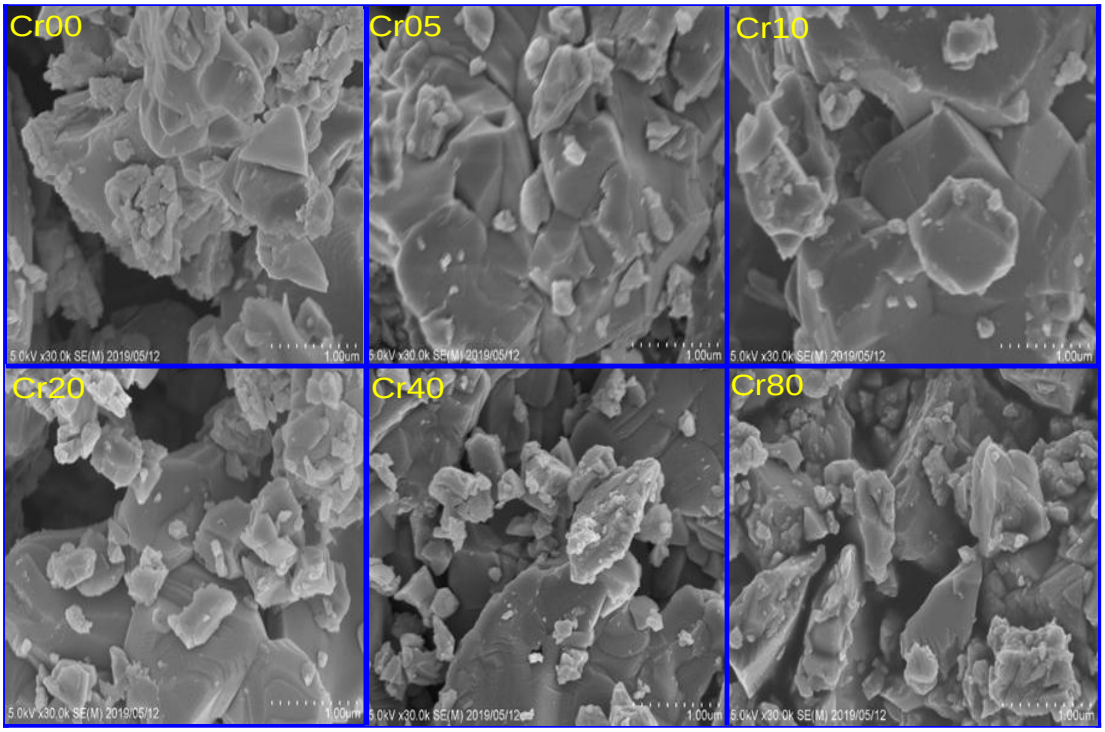

Fig. (4): The SEM images of $Cd_{0.5}Cu_{0.5}Cr_xFe_{2-x}O_4$ nanoferrite samples

DC measurement

The temperature dependency of the σ_{dc} of the Cr ferrites has been studied. An exponentially increasing value of σ_{dc} with temperature was observed according to the following Arrhenius relation **(Assar and Abosheiasha, 2015)**:

$$\sigma_{dc} = \sigma_0 e^{-Ea/KT} \quad (8)$$

; where σ_0 is a pre-exponential factor in the dimension of (S/cm), K is Boltzmann's constant, E_a is the activation energy, and T is the absolute temperature. In fact, the electrical conduction in a material depends essentially on the way of production of charge carriers and their transport in that material. It may be interpreted by Verwey's hopping mechanism **(Hashim *et al.*, 2014)**.

Accordingly, in ferrites, the σ_{dc} is primarily owing to the hopping electron among ions of the same elements in many valence states and distributed randomly through the same sub-lattices.

Based on the crystal structure of spinel ferrites, the cations populate the tetrahedral A-sites and octahedral B-sites of a cubic close-packed oxygen lattice. In view of the fact that the Fe^{3+} ions are mainly present at A-sites and Fe^{2+} ions generated even during the preparation process tend to populate B-sites exclusively, there are not any charge carriers hopping between A-A sites. B-B hopping has a far higher probability of

occurring than A-B hopping since the separation between two metal ions on B-A sites is wider than on B-B sites. The ion separation distance and the activation energy required for charge carrier hopping, correspondingly, are considered to be based on the hopping probability in B-sites. Charges may migrate in B-sites due to an applied electric field, influencing the electric signal of spinel ferrites **(Gupta *et al.*, 2018)**. The plot of the Arrhenius relation of the σ_{dc} of the investigated samples from the room temperature up to 490K ($\ln(\sigma_{dc})$ vs. *1000/T*) is displayed in **Fig. (5)**. It can be shown that $\ln(\sigma_{dc})$ of all the samples increased linearly with the increase of temperature showing a semiconducting behavior. The activation energy values versus Cr concentration increased where the activation energy was in the range of 0.349 - 0.407 eV (as mentioned in Table 4). It can be noticed that increasing doping content decreases conductivity σ_{dc}. This increase in activation energy implies that the Cr ions taking part in octahedral sites hinder the electron hopping between $Fe^{3+} \leftrightarrow Fe^{2+}$ ions lowering electrical conduction by obstructing Fe^{2+} and Fe^{3+} alteration **(Kumar, Sridhar and Ravinder, 2018)**.

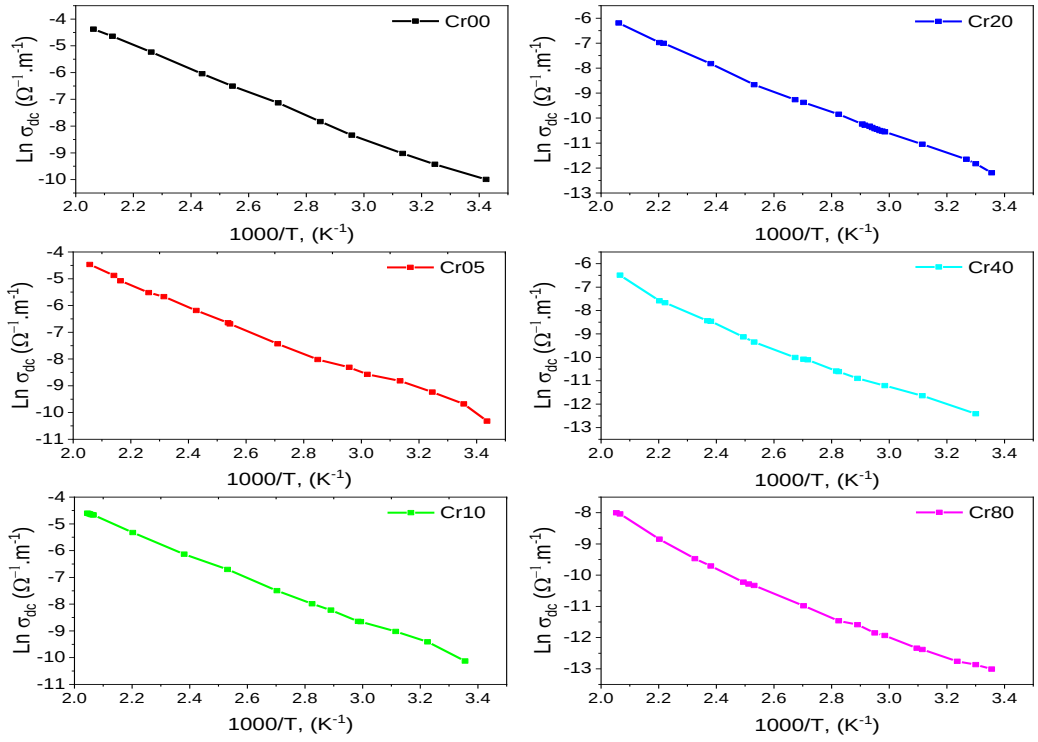

Fig. (5): Temperature dependence of the σ_{dc} for the $Cd_{0.5}Cu_{0.5}Cr_xFe_{2-x}O_4$ nanoferrite samples

The values of activation energy E_a are inversely related to conductivity (by decreasing conductivity, the activation energy E_a increases), as reported by S. Yonatan Mulushoa et al. **(Mulushoa *et al.*, 2018)**.

Table (4): DC electrical parameters (E_a and σ_{dc}) of $Cd_{0.5}Cu_{0.5}Cr_xFe_{2-x}O_4$ nano ferrites samples.

Sample	E_a (eV)	σ_{dc} (Ω^{-1}. cm^{-1})
Cr00	0.375	7.34×10^{-7}
Cr05	0.349	6.26×10^{-7}
Cr10	0.364	3.99×10^{-7}
Cr20	0.398	5.06×10^{-8}
Cr40	0.407	2.41×10^{-8}
Cr80	0.398	2.24×10^{-8}

Conclusion

Cr-substituted Cd-Cu ferrite samples were successfully produced using the co-precipitation technique. The crystallization of the samples results in cubic crystal symmetry (space group Fd3m). It has been found that as Cr^{3+} content increases, the lattice parameter *a*, experimental density D_{exp}, and x-ray density D_x decrease while the porosity *P* of the samples increases. For the five phases of weight reduction, the Horowitz and Metzger technique was used to compute the average decomposition energy E_d of the degradation in the TGA study. The SEM images indicate that increased doping ion concentration causes high agglomeration and clustering, which may be induced by oxygen vacancies and porosity restricting grain dispersion. DC Conductivity σ_{dc} of the materials can be explained by the hopping process between Fe^{3+} and Fe^{2+} through oxygen. By increasing Chromium Cr^{3+} content, the electrical conductivity σ_{dc} decrease due to the replacement process of Cr^{3+} for Fe^{3+}, resulting in the lower of Fe^{3+} ions at the B-site. The activation energy E_a of charge carriers' hopping rises as Cr^{3+} concentration increases. All these changes are favorable for electronic applications.

Reference

M. A. Amer, A. Matsuda, G. Kawamura, R. El-Shater, T. Meaz and F. Fakhry, *J. Magn. Magn. Mater.*, 2017, **439**, 373–383.

M. N. Ashiq, F. Naz, M. A. Malana, R. S. Gohar and Z. Ahmad, *Mater. Res. Bull.*, 2012, **47**, 683–686.

S. T. Assar and H. F. Abosheiasha, *J. Magn. Magn. Mater.*, 2015, **374**, 264–272

R. E. El-Shater, *Chinese J. Phys.*, , DOI:10.1016/j.cjph.2018.10.028

R. E. El-Shater, H. El Shimy and S. T. Assar, *Mater. Chem. Phys.*, 2020, **247**, 122758.

R. Ghasemi, J. Echeverría, J. I. Pérez-Landazábal, J. J. Beato-Lopez, M. Naseri and C. Gómez-Polo, *J. Magn. Magn. Mater.*, 2020, **499**, 166201.

Gul H, A.-H. A. Shah, S. Gul, J. Arjomandi and S. Bilal, *Iran. J. Chem. Chem. Eng.*, 2018, **37**, 193–204.

M. Gupta, Anu, R. K. Mudsainiyan and B. S. Randhawa, *Mater. Sci. Eng. B*, 2018, **227**, 1–8.

M. Hashim, Alimuddin, S. E. Shirsath, R. K. Kotnala, S. S. Meena, S. Kumar, A. Roy, R. B. Jotania, P. Bhatt and R. Kumar, *J. Alloys Compd.*, 2013, **573**, 198–204.

M. Hashim, S. S. Meena, R. K. Kotnala, S. E. Shirsath, A. S. Roy, A. Parveen, P.

Bhatt, S. Kumar, R. B. Jotania, R. Kumar and Alimuddin, *J. Alloys Compd.*, 2014, **602**, 150–156.

P. Jadoun, J. Sharma, S. Kumar, S. N. Dolia, D. Bhatnagar and V. K. Saxena, *Ceram. Int.*, 2018, **44**, 6747–6753.

H. Kaur, A. Singh, V. Kumar and D. S. Ahlawat, *J. Magn. Magn. Mater.*, 2019, **474**, 505–511.

K. A. M. Khalaf, A. D. Al-Rawas, H. M. Widatallah, K. S. Al-Rashdi, A. Sellai, A. M. Gismelseed, M. Hashim, S. K. Jameel, M. S. Al-Ruqeishi, K. O. Al-Riyami, M. Shongwe and A. H. Al-Rajhi, *J. Alloys Compd.*, 2016, **657**, 733–747.

K. V. Kumar, R. Sridhar and D. Ravinder, *Process. Appl. Ceram.*, 2018, **12**, 1–7.

H. S. Lokesha, P. Mohanty, A. R. E. Prinsloo and C. J. Sheppard, 2021.

S. F. Mansour, M. A. Abdo and S. M. Alwan, *Ceram. Int.*, 2018, **44**, 8035–8042.

S. Y. Mulushoa, N. Murali, M. T. Wegayehu, S. J. Margarette and K. Samatha, *Results Phys.*, 2018, **8**, 772–779.

S. R. Naik, A. V Salker, S. M. Yusuf and S. S. Meena, *J. Alloys Compd.*, 2013, **566**, 54–61.

S. Supriya, S. Kumar and M. Kar, *J. Mater. Sci. Mater. Electron.*, 2017, **28**, 10652–10673.

S. Uday Bhasker, Y. Veeraswamy, N. Jayababu and M. V. Ramanareddy, *Mater. Today Proc.*, 2016, **3**, 3666–3672.

M. Vadivel, R. R. Babu, K. Sethuraman, K. Ramamurthi and M. Arivanandhan, *J. Magn. Magn. Mater.*, 2014, **362**, 122–129.

W. Wang, Z. Ding, X. Zhao, S. Wu, F. Li, M. Yue and J. P. Liu, *J. Appl. Phys.*, 2015, **117**, 6–10.

A. Yadav, P. Choudhary, P. Saxena, V. N. Rai and A. Mishra, *J. Adv. Dielectr.*, 2019, **9**, 1–12.

الخصائص الحرارية والكهربائية لعينات الكادميوم - النحاس الفريتات النانوية المطعمه بالكروم

احمد وحيد عوض[١*] ،رضا السيد الشاطر[١] ،هاني حمدي البهنساوي[٢] ،طلعت محمد ميز[١]

١ قسم الفيزياء ، كلية العلوم ، جامعة طنطا ، ٣١٥٢٧ ، مصر
٢ قسم الفيزياء ، كلية العلوم ، جامعة الأزهر ، مدينة نصر ١١٨٨٤ ، القاهرة ، مصر

تم تصنيع مواد الفريت النانويه لعينات الكادميوم - النحاس المطعمه بالكروم بنجاح بواسطة تقنية الترسيب المشترك. تم استخدام قياسات الاشعه السينيه و التحليل الوزني الحراري و التيار المستمر الكهربي لتحديد خواص العينات المصنعه. وفقًا لتحليل الاشعه السينيه ، فإن العينات المصنعه لها تركيب بلوري مكعب الشكل. يتراوح الحجم البلوري في المدي ١٤,٨-٢٢,٦ نانومتر. متوسط طاقات التحلل للمراحل الأربع لفقدان الوزن من التحلل كما هو مبين من خلال الرسوم البيانية للتحليل الوزني الحراي هي ١,٣٩ ، ٦,٥٣ ، ٣٩,١٤ ، و ٢١,٤٠ (كيلوجول / مول). انخفضت توصلية درجة حرارة الغرفة تدريجياً من 7.34× 10^{-7} $\Omega^{-1}.cm^{-1}$ لعينة Cr00 إلى ٢,٢٤ × ١٠$^{-8}$ $\Omega^{-1}.cm^{-1}$ للعينة Cr80. تم استنتاج قيم طاقة التنشيط في المدي من ٠,٣٤٩ الي٠,٤٠٧ فولت. تُظهر التوصلية الكهربائية المعتمدة على درجة الحرارة لجميع العينات سلوكًا يشبه أشباه الموصلات. نتيجة لذلك ، قد تكون المواد المصنعه مناسبة للحد من الفقد تيارات الدوامية.